NASA Technical Paper 2241

February 1984

Threshold Kinetics of a Solar-Simulator-Pumped Iodine Laser

John W. Wilson,
Yeunggil Lee,
Willard R. Weaver,
Donald H. Humes,
and Ja H. Lee

NASA

NASA Technical Paper 2241

1984

Threshold Kinetics of a Solar-Simulator-Pumped Iodine Laser

John W. Wilson
Langley Research Center
Hampton, Virginia

Yeunggil Lee
Hampton Institute
Hampton, Virginia

Willard R. Weaver
and Donald H. Humes
Langley Research Center
Hampton, Virginia

Ja H. Lee
Vanderbilt University
Nashville, Tennessee

National Aeronautics
and Space Administration

Scientific and Technical Information Branch

CONTENTS

INTRODUCTION

The atomic iodine laser based on the photodissociation of alkyl iodide gases was among the first proposed for direct solar-to-laser energy conversion in space (ref. 1). The first solar-simulator demonstration being achieved (ref. 2), more attention is now given to system requirements of chemical reversibility and lasant reprocessing in scaling to large space systems. Such a scaling requires an adequate knowledge of the chemical processes present in the gas during laser operation (ref. 3). The development of a preliminary chemical kinetic model is presented elsewhere with limited comparison to solar simulator experiments (ref. 4).

It was shown in a previous report (ref. 4) that the laser output consists of a transient pulse region followed by a continuous wave (cw) region in which the laser power output is proportional to the power absorbed. At late times, the cw region is terminated as a result of quenching by the iodine molecule which formed through three-body collision of two ground-state iodine atoms with an alkyl iodide molecule. The I_2 formation critically depends on the reaction rates of the alkyl iodide recombination

$$R + I \rightarrow RI$$

and three-body formation of I_2 as

$$I + I + RI \rightarrow I_2 + RI$$

where R denotes the alkyl radical. It was determined (ref. 4) that some of the rate constants for these reactions in the literature are not compatible with Langley experiments.

In the present report, the kinetic factors involved in reaching laser threshold are examined. In particular, the effects of gas diffusion, hyperfine splitting, and gain length scaling are treated in detail.

SOLAR SIMULATOR

The solar-simulator light source is an arc discharge across an 8-mm gap stabilized by a 1030-kPa (10.2-atm) Xe flow. The light output is reflected by a high-quality elliptical reflector and focused in the chopper plane as shown in figure 1. The reflector has a vapor-deposited aluminum front surface protected by a MgF_2 coating to prevent surface oxidation and abrasion. The spectral content of the arc plasma output corresponds to blackbody emission at 6000 K at the focus of the elliptical reflector. The divergent light beam leaving the focus is collected by a 7075 aluminum alloy 25° cone with a polished interior surface and MgF_2 coating. The light beam is again focused on the cone axis, which is aligned with the optical axis of the system. Three different cone sizes were used to gain scaling information for model testing.

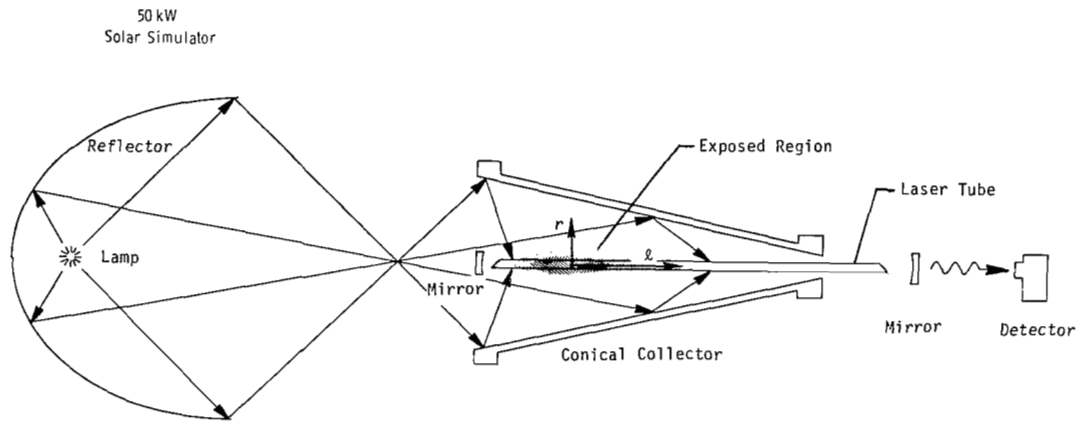

Figure 1.- Setup for solar-simulator-pumped laser experiment.

The photon flux on the wavelength interval between λ and $\lambda + d\lambda$ emitted by a blackbody radiator at a temperature T is

$$\phi(\lambda)\, d\lambda = \frac{2\pi c}{\lambda^4} \frac{d\lambda}{\exp(hc/\lambda kT) - 1} \tag{1}$$

where c is the velocity of light, h is Planck's constant, and k is Boltzmann's constant. The exponential argument is given as

$$\frac{hc}{k\lambda T} = \frac{1.44}{\lambda T} \tag{2}$$

for λ in centimeters and T in kelvin. The light is reflected from the conic collector with a reflectance R_λ at each wavelength before reaching the optical axis. The light intensity at the optical axis is related to the geometry of the arc plasma and the reflector and collector surfaces, denoted by the function $M(r,\ell)$, as

$$I_\lambda(r,\ell)\, d\lambda = M(r,\ell)\, R_\lambda \varepsilon_\lambda\, \phi(\lambda)\, d\lambda \tag{3}$$

where ε_λ is the photon energy.

The light intensity is measured by a calorimeter and represented by

$$C(r,\ell) = C_o' \exp\left[-2.77\left(\frac{\ell^2}{L^2} + \frac{r^2}{R^2}\right)\right] \tag{4}$$

where C_o' is the peak intensity of the arc image, L is the full length at half maximum light intensity along the tube axis, R is the full width at half maximum light intensity transverse to the tube axis, ℓ is the distance along the tube axis, and r is the distance from the tube axis. The size of the arc image depends on the size of the cone collector and its distance from the focus. It is clear that

$$C(r,\ell) = \int_0^\infty M(r,\ell)\, R_\lambda \varepsilon_\lambda\, \phi(\lambda)\, d\lambda \tag{5}$$

which allows $M(r,\ell)$ to be determined from the calorimeter data. Since most of the energy is in the visible region where R_λ is nearly constant, equation (5) may be written with the help of equation (4) as

$$M(r,\ell) = \frac{C_o' \exp\left[-2.77\left(\ell^2/L^2 + r^2/R^2\right)\right]}{R_{vis} \int_0^\infty \varepsilon_\lambda\, \phi(\lambda)\, d\lambda} \tag{6}$$

where R_λ is replaced by the constant R_{vis}, since mainly visible radiation contributes to the calorimeter measurements. Expressing the numerator and denominator in units of the solar constant yields

$$M(r,\ell) = \frac{C_o \exp\left[-2.77\left(\ell^2/L^2 + r^2/R^2\right)\right]}{R_{vis}} \tag{7}$$

where it is found from the calorimeter data that

$$C_o = \frac{2.72 \times 10^4}{(1 + 0.375m)^2} \tag{8}$$

$$L = \frac{(4 + 1.5m)(m + 5)}{8} \tag{9}$$

$$R = \frac{2.192 + 0.824m}{5 + m} \tag{10}$$

and m is a parameter associated with the scale of the three collector cones with different apertures. (See table I.)

TABLE I.- SCALE PARAMETERS FOR COLLECTOR CONES

Aperture diameter, cm	Distance from focus, cm	m	C_o, solar constants	L, cm	R, mm
9.6	7.0	0.5	19 288	3.27	4.73
16.6	15.2	2.0	8 881	6.13	5.49
23.6	24.5	2.5	7 245	7.27	5.67

A comparison between measurements of intensity along the optical axis and the model function of equation (4) in units of the solar constant is shown in figure 2. Measurements in the radial direction for the cone with an aperture diameter of 16.6 cm at a location 3 cm along the optical axis from the peak intensity are shown in figure 3 in comparison with a theoretical curve based on equation (4).

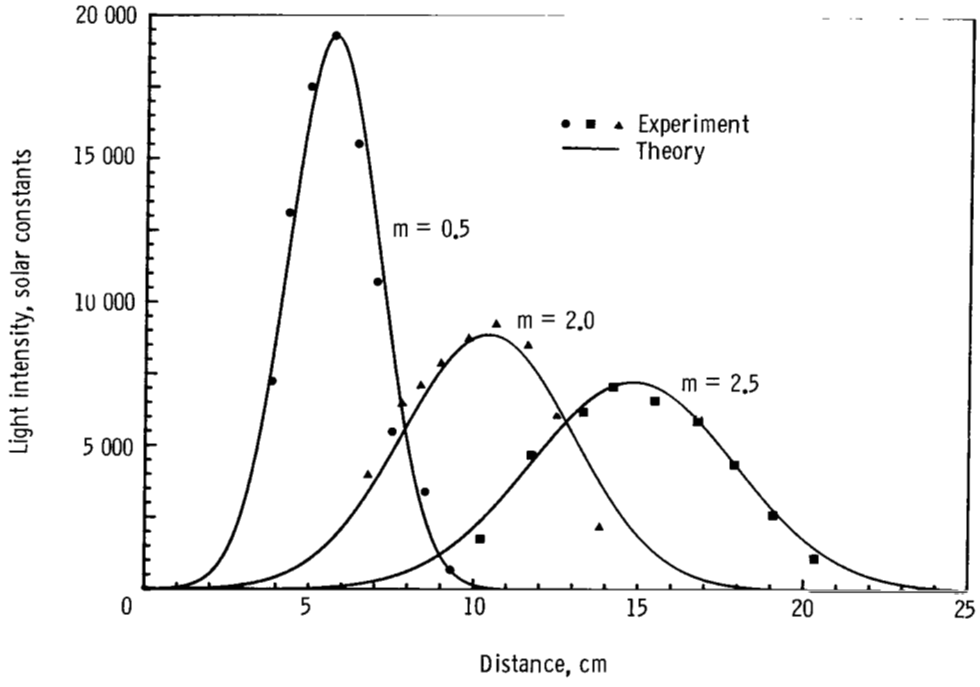

Figure 2.- Illumination on axis of laser tube as a function of distance behind cone face. Curve is based on equation (4) and table I. Dots are experimental measurements of April 13, 1981 (aperture with 9.6-cm diameter). Triangles are experimental measurements of July 30, 1981 (aperture with 16.6-cm diameter). Squares are experimental measurements of March 25, 1981 (aperture with 23.6-cm diameter).

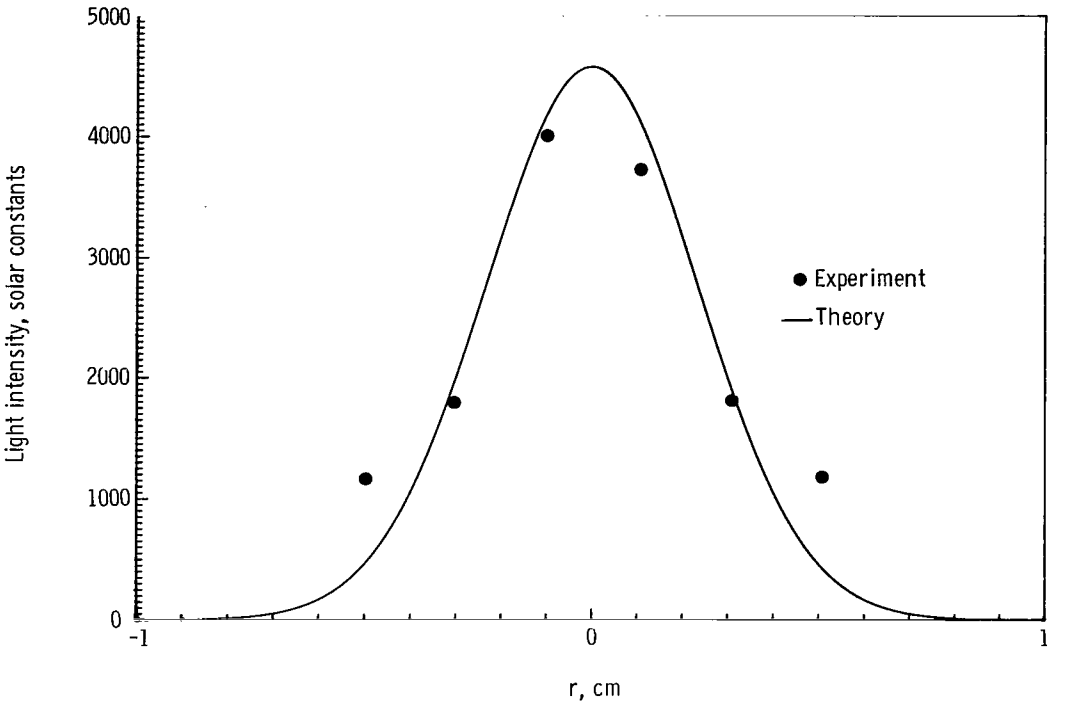

Figure 3.- Illumination as a function of distance from cone axis (16.6-cm-diameter aperture). Curve is based on equation (4) and table I. Dots are experimental measurements of July 30, 1981.

Although the lamp intensity is presented as a static quantity, there are, in fact, a number of poorly understood factors that affect the illumination of the central region of the collector cone. Because the lamp electrodes are mechanically held in place, slow erosion will widen the gap and cause a less localized arc. The installation of new lamps will not restore the machine to its initial operation because of lamp differences. In addition, there are unknown factors causing day-to-day variations in the measured illumination. Aside from these long-term variations, there are small temporal fluctuations in the arc plasma which cause large spatial movements in the arc image because of the large magnification factors. This produces some difficulty in interpretation of the laser experiments, since the instantaneous pump power is generally less than its maximum. Only by considering many experimental runs can the ideal experimental result (that is, result corresponding to maximum pump power) be identified.

The light is reflected by the conic collector and concentrated on the cone axis with intensity given by equation (3). The laser tube is centered on the cone axis for which the peak light intensity crosses the tube wall at an angle of 46° before reaching the lasant gas. (See fig. 4.) The reflection loss at the tube interfaces is $R_t \approx 0.08$, and the transmission through the 1-mm quartz tube is near unity. The attenuation of the light in passing through the filling gas to the laser tube centerline is

$$\Phi_\lambda(x) = \exp[-n\,\sigma(\lambda)\,x]\,R_t\,M(0,\ell)\,R_\lambda\,\phi(\lambda)\,d\lambda \qquad (11)$$

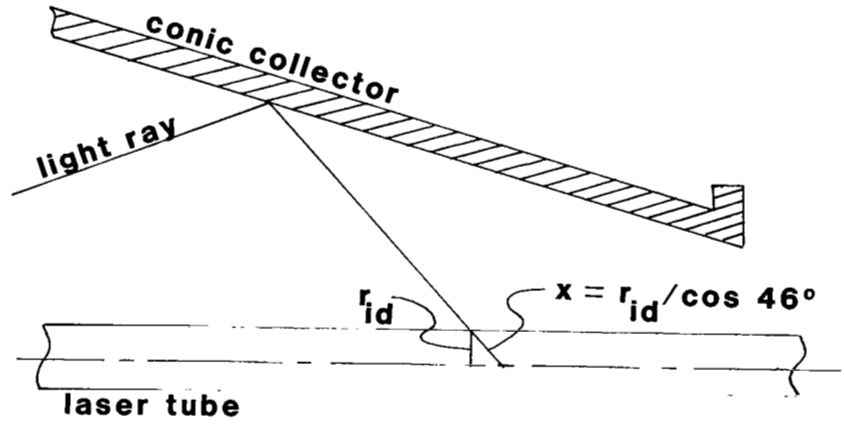

Figure 4.- Typical light ray reflected into laser tube.

where x is the slant distance (see fig. 4) from the centerline to the inner tube surface along the light path ($x \approx r_{id}/\cos 46°$), n is the number density of the specific absorbing gas molecule, and

$$\sigma(\lambda) = \sigma_o \exp\left[\frac{-(\lambda - \lambda_o)^2}{4\delta_o^2}\right] \tag{12}$$

is the specific photoabsorption cross section with peak cross section σ_o, line center λ_o, and line width δ_o given in table II according to references 5 to 7. Of the photons absorbed in the spectral region of equation (12), the absorbing molecules are fragmented to yield atomic iodine. The two alkyl iodides and I_2 photodissociate into fractions Φ_{I^*} of metastable iodine with values of 100 percent and 51 percent, respectively. (See table II.)

TABLE II.- PHOTOABSORPTION PARAMETERS USED FOR THE EQUIVALENT POWER OF ONE SOLAR CONSTANT EXPOSURE, 1.4 kW/m^2

Parameter	$n\text{-}C_3F_7I$ (ref. 5)	$i\text{-}C_3F_7I$ (ref. 6)	I_2 (ref. 7)
σ_o, cm^2	7.9×10^{-19}	6.2×10^{-19}	9.14×10^{-19}
λ_o, nm	272	275	499
δ_o, nm	12.7	14.5	23.0
Φ_{I^*}	1.0	1.0	0.51
S, sec^{-1}	3.04×10^{-3}	3.37×10^{-3}	3.38×10^{-2}
R_{λ_o}/R_{vis}	0.8	0.8	1.0
f	0.652	0.653	0.673

The rate at which I* is formed in the laser tube is

$$\xi(r,\ell) = \int_0^\infty \Phi_{I^*} n\, \sigma(\lambda)\, R_t\, M(r,\ell)\, R_\lambda \exp[-n\, \sigma(\lambda)\, x]\, \phi(\lambda)\, d\lambda$$

$$\xi(r,\ell) = \Phi_{I^*} n R_t\, M(r,\ell) \int_0^\infty R_\lambda\, \sigma(\lambda) \exp[-n\, \sigma(\lambda)\, x]\, \phi(\lambda)\, d\lambda \tag{13}$$

which is evaluated through approximation with Gauss-Hermite quadrature (ref. 8) and yields

$$\xi(r,\ell) = 2\delta_o \Phi_{I^*}\, n\sigma_o R_t R_{\lambda_o}\, M(r,\ell) \left\{1.18\, \phi(\lambda_o) \exp(-n\sigma_o x)\right.$$

$$\left. + 2.95\left[\phi(\lambda_o + 2.45\delta_o) + \phi(\lambda_o - 2.45\delta_o)\right] \exp(-0.223 n\sigma_o x)\right\} \tag{14}$$

Equation (14) may now be simplified as

$$\xi(r,\ell) = \frac{R_t R_{\lambda_o}}{R_{vis}} Sn[f \exp(-n\sigma_o x) + (1 - f) \exp(-0.223 n\sigma_o x)]\, C(r,\ell) \tag{15}$$

where S (maximum photodissociation rate) and f (fractional absorption near line center) are given in table II. The usefulness of the Hermite quadrature is demonstrated in figure 5 where equation (15) is compared with an accurate numerical evaluation of equation (13) and the usual exponential approximation.

ENERGY LEVELS AND REACTION PRODUCTS

There are several chemical/physical processes important to the formation and loss of excited iodine. Several requirements must be met in order that specific reactions may occur. The first such requirement is that the change in internal energy be less than or on the order of the average thermal energy.

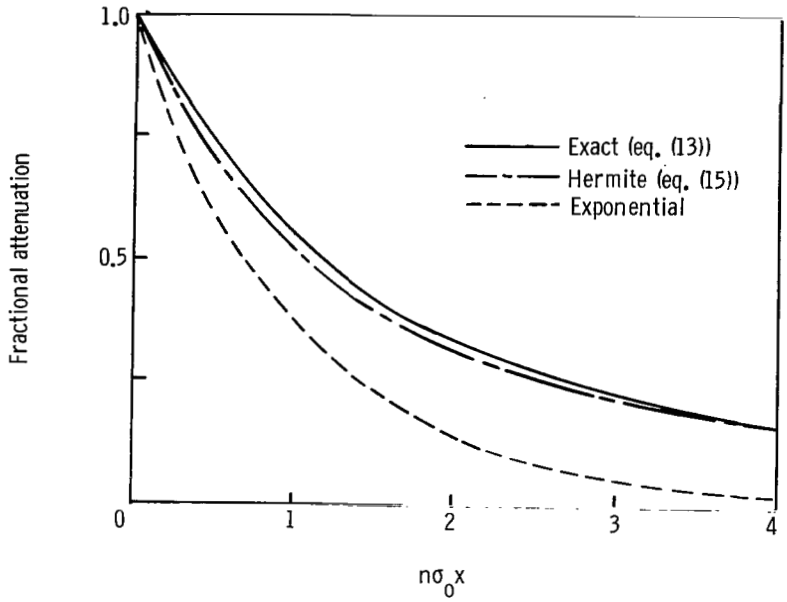

Figure 5.- Relative attenuation of light as a function of penetration into lasant gas ($n\text{-}C_3F_7I$).

Molecular Fragmentation

The approximate bond energies of the alkyl iodide constituents are given in table III. These energies are mean molecular values compiled by Huheey (ref. 9).

TABLE III.- SINGLE- AND DOUBLE-BOND ENERGIES AND DISTANCES OF ALKYL IODIDE CONSTITUENTS

[From ref. 9]

Bond	Bond energy, D_o, eV	Bond distance, r, pm
C-C	3.58	154
C=C	6.24	134
F-F	1.60	142
I-I	1.54	267
C-F	5.03	135
C-I	2.21	214
I-F	2.88	191

First consider the ways in which the basic $CF_3CF_2CF_2I$ molecule could fragment and the corresponding enthalpies as shown in table IV. The fragments are ordered according

TABLE IV.- $CF_3CF_2CF_2I$ FRAGMENTATION PRODUCTS AND CORRESPONDING ENTHALPIES

Reaction product	ΔH, eV/mol
$CF_4 + CF_2CFI$	0.92
$C_2F_4 + CF_3I$	.92
$CF_2CFCF_3 + IF$	1.70
$\bullet CF_2CF_2CF_3 + I$	2.21
$\bullet CF_3 + \bullet CF_2CF_2I$	3.58
$\bullet CF_2CF_2CF_2I + F$	5.03
$CF_2CFCF_2I + F_2$	5.80

to increasing enthalpies so that the most likely fragments appear at the top of the table. It is clear that none of these products should be present during ordinary room temperature chemical processes, although photofragmentation or other energetic processes could potentially form some of the listed fragments. There are no absorption bands in the visible region (ref. 10) which could give rise to the products listed. Thus, they could be directly formed only at pump rates with heat release sufficient for pyrolytic decomposition. Many of these fragments have been observed in pyrolysis studies (ref. 11). It is anticipated that pyrolysis will not be important in the present study, since relatively small energy deposits are sufficient to excite the gas to threshold. Photofragmentation will, of course, be of major importance.

Photodissociation Products

The lowest order photodissociation process in the perfluoroalkyl iodides corresponds to the electronic excitation of a nonbonding electron of the iodine to an antibonding (π^*) orbital (ref. 10). A similar transition occurs in the fluorine but only for hard ultraviolet (UV) photons. The potential energy curves along the C-I bond direction are shown in figure 6. The curves were drawn using the Morse function for the ground-state potential with the spring constant according to Badger's relation (ref. 12). The repulsive antibonding potential is approximated by

$$V_\pi(r) = \varepsilon^* + D_o + A \exp[-a(r - r_c)] \tag{16}$$

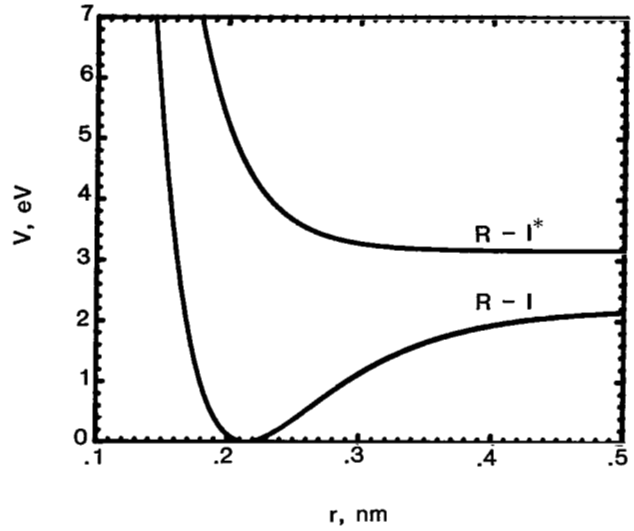

Figure 6.- Potential along R-I bond direction.

where $\varepsilon^* = 0.94$ eV is the $I(^2P_{1/2})$ excitation energy; D_o is the C-I bond energy; r is the C-I separation; and the parameters A, a, and r_c are determined from the photodissociation parameters λ_o and δ_o in table II. The photodissociation is predominantly into the iodine metastable state (I*) (ref. 13)

$$RI + h\nu_o \rightarrow R + I^*$$

where ν_o is the central frequency, and the potential energy between the fragments immediately after photoabsorption is ≈1.39 eV. The resultant kinetic energies of the R and I* fragments are 0.60 and 0.79 eV, respectively. It is not anticipated that the photodissociation of I_2 will ever play a major role in production of I or I*, since I_2 is a serious quenching molecule and quickly halts laser operation. Clearly, the major constituents in addition to the lasant gas to be found at any time in the laser tube will be the photolysis products and subsequent reaction products. The possible reactions of the photolysis products must now be examined.

Primary Reactions

The possible reactions of the lasant molecules and the photodissociation products are given in table V in the order of increasing enthalpies. The last two reactions of table V are unimportant because of the large energy input required, and the

$$I^* + I^* \rightarrow I_2$$

reaction is omitted because recombination is along a highly repulsive potential surface. The exciplex formation

$$I^* + RI \rightarrow RI_2^*$$

TABLE V.- PRINCIPAL REACTIONS OF PHOTODISSOCIATION PRODUCTS AND CORRESPONDING ENTHALPIES

[R = $\bullet C_3F_7$]

Reaction	ΔH, eV/mol
$R + R \rightarrow R_2$	-3.58
$I^* + I^* \rightarrow I_2$	-3.42
$I^* + I \rightarrow I_2$	-2.48
$R + I \rightarrow RI$	-2.21
$I + I \rightarrow I_2$	-1.54
$R + RI \rightarrow R_2 + I$	-1.37
$R + I^* \rightarrow RI$	-1.27
$I^* \rightarrow I$	-.94
$RI + RI \rightarrow R_2 + I_2$	-.70
$R + RI \rightarrow R_2 + I^*$	-.43
$I^* + RI \rightarrow RI_2^*$	-.07
$I + RI \rightarrow R + I_2$	.67
$I^* + RI \rightarrow R + I_2$	1.61

is contained in the usual quenching coefficient discussed subsequently. The remaining reactions are all exothermic, and their corresponding rates are mainly limited by steric factors and activation thresholds. For example, the reaction among lasant molecules

$$RI + RI \rightarrow R_2 + I_2$$

is first highly limited by the complicated structure of the RI molecule but, in addition, has a threshold approaching 4 eV. In fact, this reaction seems to play, at most, a minor role in pyrolytic decomposition (ref. 11).

The recombination

$$R + R \rightarrow R_2$$

has no threshold and is mainly delayed by steric factors, as is

$$R + I \rightarrow RI$$

The excess kinetic energy in both reactions is absorbed by the internal energy of the alkyl radicals so that a third body is not required.

The important reaction for lasers

$$R + I^* \rightarrow RI$$

is inhibited by the repulsive potential (fig. 6) between them. This reaction is the principal loss of excited iodine and the main limit in reaching laser threshold.

Loss of the electronic excitation energy through various collisional processes denoted by

$$I^* \rightarrow I$$

is the ultimate limiting factor in the laser operation. Such losses occur through collisional energy transfer, exciplex formation, and collision with the wall. Radiative decay plays a minor role because of the long lifetime of this metastable state.

The formation of molecular iodine is a three-body reaction; the third body is needed to stabilize the reaction by absorbing kinetic energy to extract the excess energy of translational motion. These reactions

$$I + I \rightarrow I_2$$

and

$$I^* + I \rightarrow I_2$$

are particularly important to laser operation because the high quenching rate of the iodine molecule is the main limit to laser pulse duration and processing of used lasant material.

Secondary Reactions

The possible secondary reactions of the new species formed through the primary reactions are shown in table VI. Of these, only two reactions appear to be of any potential importance. The first,

$$R + I_2 \rightarrow RI + I$$

is suppressed by steric factors as well as activation energy on the order of 1 eV. If this reaction occurs, it is probably only among hot radicals produced in the photodissociation of the lasant molecules. The second reaction,

$$I^* + R_2 \rightarrow RI + R$$

is inhibited by an approximate 2-eV threshold and poor electronic-to-vibration coupling. This reaction and subsequent reactions in table VI are unimportant.

TABLE VI.- SECONDARY REACTIONS AND CORRESPONDING ENTHALPIES

[R = $\bullet C_3F_7$]

Reaction	ΔH, eV/mol
$R + I_2 \rightarrow RI + I$	-0.67
$I^* + R_2 \rightarrow RI + R$	.43
$I_2 + R_2 \rightarrow 2RI$	.70
$I + R_2 \rightarrow RI + R$	1.37

CHEMICAL REACTION RATES

The specific reaction rates of the reactions which appear possible under simple energy considerations must be known before a complete chemical kinetic model can be derived. Specific reaction rate data are collected and summarized in this section. The symbols for the reaction rate coefficients are defined in table VII.

TABLE VII.- MEAN REACTION RATE COEFFICIENTS AND ASSOCIATED UNCERTAINTY FACTORS BASED ON LITERATURE VALUES

[The factor in parentheses gives the uncertainty limits associated with the coefficient]

Reactants	Products	Reaction rate coefficient, $(cm^3)^n/sec$		
		Symbol	$R = n\text{-}C_3F_7$	$R = i\text{-}C_3F_7$
R + R	R_2	K_3	2.6×10^{-12} $(4)^{\pm 1}$	9.0×10^{-13} $(3.8)^{\pm 1}$
R + I	RI	K_2	2.3×10^{-11} $(3.5)^{\pm 1}$	3.9×10^{-11} $(4.3)^{\pm 1}$
I + I + RI	I_2 + RI	C_2	8.5×10^{-32} $(5.3)^{\pm 1}$	8.3×10^{-32} $(5.3)^{\pm 1}$
I + I + I_2	I_2 + I_2	C_4	3.8×10^{-30} $(1.3)^{\pm 1}$	3.8×10^{-30} $(1.3)^{\pm 1}$
R + RI	R_2 + I	K_4	3×10^{-16}	3×10^{-16}
R + I*	RI	K_1	5.6×10^{-13} $(6.2)^{\pm 1}$	1.7×10^{-13} $(17)^{\pm 1}$
I* + RI	I + RI	Q_1	2.0×10^{-16} $(4.2)^{\pm 1}$	7×10^{-17} $(4.1)^{\pm 1}$
I* + I_2	I + I_2	Q_2	1.9×10^{-11} $(2.6)^{\pm 1}$	1.9×10^{-11} $(2.6)^{\pm 1}$
I* + I + RI	I_2 + RI	C_1	3.2×10^{-33} $(3.2)^{\pm 1}$	3.2×10^{-33} $(3.2)^{\pm 1}$
I* + I + I_2	I_2 + I_2	C_3	8×10^{-32} $(1.8)^{\pm 1}$	8×10^{-32} $(1.8)^{\pm 1}$
R + RI	R_2 + I*	K_5	3.2×10^{-17} $(3.2)^{\pm 1}$	3.2×10^{17} $(3.2)^{\pm 1}$
I* + RI	RI_2^*	K_6	8.3×10^{-18} $(1.3)^{\pm 1}$	6.5×10^{-18} $(1.1)^{\pm 1}$

Reaction Rate for $R + R \rightarrow R_2$

The reaction rate coefficient for $R + R \rightarrow R_2$ is given for CF_3 radicals to be 1.1×10^{-11} cm^3/sec by Hohla and Kompa (ref. 14). It is expected to be slower for C_3F_7 because of steric factors, although the additional degrees of freedom tend to stabilize this two-body reaction. This value was likewise adopted by Turner and Rapagnani (ref. 15). Further studies were made by Kuznetsova and Maslov (ref. 16) on the normal and isomeric forms of the radical and with varying degrees of saturation of the gain medium. They find a value of 3.19×10^{-12} cm^3/sec within a factor of 3.8 for the normal form and 7.7×10^{-13} cm^3/sec within a factor of 3.1 for the isomeric form. Later studies using transverse electron discharge excitation yielded 4.2×10^{-12} cm^3/sec for $i\text{-}C_3F_7$ (ref. 17). Values for recombination are given by Fisk (ref. 18) as 6×10^{-13} cm^3/sec for $n\text{-}C_3F_7$ and 1.5×10^{-12} cm^3/sec for $i\text{-}C_3F_7$, although his logic in arriving at these values is not detailed. The uncertainty in Kuznetsova and Maslov's original estimates was greatly reduced in their later work (ref. 19) with no substantial disagreement with their earlier values (ref. 16).

Later measurements of Skorobogatov and Slesar (ref. 20) yielded the value of 1.77×10^{-12} cm^3/sec for $i\text{-}C_3F_7$. The values adopted for this study are shown in table VII.

Reaction Rate for R + I → RI

The principal reaction by which the lasant material is recovered is R + I → RI. The rate proposed by Hohla and Kompa (ref. 14) and used by Turner and Rapagnani (ref. 15) is 5×10^{-11} cm^3/sec. The value obtained by Kuznetsova and Maslov (ref. 16) is 2.8×10^{-11} cm^3/sec for both $n\text{-}C_3F_7$ and $i\text{-}C_3F_7$ within a factor of 3.1. The value found according to Skorobogatov et al. (ref. 21) is 1.5×10^{-10} cm^3/sec within a factor of 3, which is equal to the value found by Beverly and Wong (ref. 17). The more recent values of Kuznetsova and Maslov (ref. 19) are somewhat lower than their earlier value. Their rate coefficients are 0.7×10^{-11} cm^3/sec for $n\text{-}C_3F_7$ and 0.6×10^{-11} cm^3/sec for $i\text{-}C_3F_7$ with an uncertainty factor of 1.15. A more recent value of Skorobogatov and coworkers (ref. 20) is 3.1×10^{-11} cm^3/sec for $n\text{-}C_3F_7$. The value 2.3×10^{-11} cm^3/sec is adopted for $n\text{-}C_3F_7$ with an uncertainty factor of 3.5, and the value 3.9×10^{-11} cm^3/sec is adopted for $i\text{-}C_3F_7$ with an uncertainty factor of 4.3, as shown in table VII.

Reaction Rate for I + I → I_2

The reaction I + I → I_2 is important because it competes with the regeneration of the lasant gas, and most importantly, the product is a serious quencher of the upper laser level (ref. 22). The iodine atoms approach along an attractive potential in the $^1\Sigma$ state but must be stabilized by collision with a third body. The $^3\pi$ state has a weak repulsive potential allowing for close approach of the two iodine atoms with collisional transitions to the $^1\Sigma$ state being likely through a third body. The efficiency of the stabilization is dependent on the mass ratio of the third body to the iodine atom and the van der Waals force of the third body. There is a rough inverse correlation between boiling point of the third-body material (that is, strong van der Waals potential) and the recombination coefficient (ref. 23).

The most important third body for solar pumping is the alkyl iodide molecule, for which the rate coefficient is taken as 4.5×10^{-31} cm^6/sec by Turner and Rapagnani (ref. 15). Measurements of Kuznetsova and Maslov (ref. 16) yielded 8.5×10^{-32} cm^6/sec for $n\text{-}C_3F_7I$ and 8.0×10^{-32} cm^6/sec for $i\text{-}C_3F_7I$. The value of 3.9×10^{-31} cm^6/sec is given by Ershov et al. (ref. 24).

The second most important third body in the gas is the I_2 molecule. The rate coefficient for this reaction is reasonably approximated as 3.8×10^{-30} cm^6/sec within a factor of 1.3 as established from references 15, 25, 26, and 27. However, this molecule must always give only a minor contribution because I_2 concentrations remain small for laser operation.

Reaction Rate for R + RI → R_2 + I

The reaction R + RI → R_2 + I is hindered by steric factors and activation energy on the order of 2 eV. Measurements of Andreeva et al. in CF_3I (ref. 28) yield a value less than 3×10^{-16} cm^3/sec.

Reaction Rate for R + I* → RI

The reaction R + I* → RI is hindered by steric factors and a repulsive potential. The value measured for CF_3 by Andreeva et al. (ref. 28) is 3.5×10^{-12} cm^3/sec, and a somewhat smaller value is expected for C_3F_7 as a result of steric factors. Kuznetsova and Maslov (ref. 16) arrive at 1.12×10^{-12} cm^3/sec within a factor of 2.9 for n-C_3F_7 and 0.5×10^{-12} cm^3/sec within a factor of 7 for i-C_3F_7. The transverse-electron-discharge-excited gas of Beverly and Wong (ref. 17) indicates a value of 2.7×10^{-12} cm^3/sec for i-C_3F_7. Later work of Kuznetsova and Maslov (ref. 19) yields the somewhat lower values of 9×10^{-14} cm^3/sec for n-C_3F_7 and 4×10^{-14} cm^3/sec for i-C_3F_7. More recently, the value of 6×10^{-13} cm^3/sec for i-C_3F_7 is given by Skorobogatov and Slesar (ref. 20), and a somewhat larger value of 3×10^{-12} cm^3/sec is found by Ershov et al. (ref. 29). Vinokurov and Zalesskii (ref. 30) suggest the rate coefficient for i-C_3F_7 to be 1×10^{-14} cm^3/sec. The value of 5.6×10^{-13} cm^3/sec with an uncertainty factor of 6.2 is assumed for n-C_3F_7, and 1.7×10^{-13} cm^3/sec with an uncertainty factor of 17 is assumed for i-C_3F_7, as shown in table VII.

Reaction Rate for I* → I

Loss of electronic excitation energy through processes other than laser oscillation is in direct competition with power generation. The loss of electronic energy can be through several processes. Thermal collisions are nearly adiabatic, so that energy transfer to translational motion is quite slow (ref. 31). The main modes of deexcitation will be energy transfer to vibrational-rotational levels and complex formation.

The deexcitation by the lasant molecules proceeds through exciplex formation

$$I^* + RI \rightarrow RI_2^* \begin{cases} \rightarrow RI + I + h\nu \\ \rightarrow RI^\dagger + I \end{cases}$$

with subsequent decay through radiation or energy transfer within the complex. The dagger superscript denotes vibrational excitation. The branching ratios have been studied (refs. 13 and 32) by observing the exciplex emission. The overall rate for

$$RI + I^* \rightarrow RI + I$$

has been measured by several groups. Turner and Rapagnani (ref. 15) recommend 8×10^{-16} cm^3/sec. Somewhat smaller values were found by Kuznetsova and Maslov (ref. 16) as 2.3×10^{-16} cm^3/sec for n-C_3F_7I and 2.8×10^{-16} cm^3/sec for i-C_3F_7I. Accurate studies of chemiluminescence by Stephan and Comes (ref. 33) and Comes and Pionteck (ref. 34) yield 4.6×10^{-17} cm^3/sec for n-C_3F_7I. A larger value, 2.0×10^{-16} cm^3/sec, was found by Dobychin et al. for n-C_3F_7I, and a much lower value, 1.7×10^{-17} cm^3/sec, was found for i-C_3F_7I (ref. 35). The values adopted are shown in table VII.

The deexcitation by I_2 is probably through the formation of a triatomic complex (ref. 36). The value adopted by Turner and Rapagnani (ref. 15) was probably influenced by the early value (5×10^{-12} cm^3/sec) given by Donovan and Husain (ref. 37). A larger value of 3.6×10^{-11} cm^3/sec is given by Beverly and Wong (ref. 17). Kartazaev et al. (ref. 38) find 2.1×10^{-11} cm^3/sec. Most of the more recent values approach 3×10^{-11} cm^3/sec (refs. 27, 36, and 39).

Reaction Rate for RI + RI → R_2 + I_2

Although the enthalpy change is easy to achieve, RI + RI → R_2 + I_2 is an unimportant reaction, inhibited by both steric factors and a high activation energy. The rate is assumed to be zero.

Reaction Rate for I* + I → I_2

The reaction I* + I → I_2 is important because it is the main source of I_2 generation before the medium is saturated. The $^3\pi$ state is attractive and easily recombines with a third body present to absorb relative translational energy in forming the bound state. The most important third body is the lasant gas, for which coefficients have been measured. Turner and Rapagnani (ref. 15) give a value of 1×10^{-33} cm^6/sec, and Beverly and Wong (ref. 17) use 1.56×10^{-32} cm^6/sec. More recently, Stephan and Comes (ref. 33) give the value 1×10^{-32} cm^6/sec. As shown in table VII, the value assumed here is the geometric midpoint 3.2×10^{-33} cm^6/sec with an uncertainty factor of 3.2, which is sufficient to span the experimental values.

The reaction as stabilized by the I_2 molecule is given as 4.3×10^{-32} cm^6/sec by Turner and Rapagnani (ref. 15) and 1.48×10^{-31} cm^6/sec by Beverly and Wong (ref. 17). The value of 8×10^{-32} cm^6/sec with an uncertainty factor of 1.8 is assumed in table VII.

Reaction Rate for R + RI → R_2 + I*

The reaction R + RI → R_2 + I* was proposed by Andreeva et al. (ref. 40) as a postphotolysis metastable production mechanism. The reaction is hindered by steric factors and a high activation energy and is most likely to proceed through hot radical reaction. Previous studies of Andreeva et al. (ref. 28) indicate this reaction to be unimportant. Direct measurements of Zalesskii and Krupenikova (ref. 41) yield the rate constant 3.2×10^{-17} cm^3/sec within a factor of 3.2. This reaction was proposed by Hohla and Kompa as a possible explanation for the postphotolysis gain increase observed in their experiments.

Reaction Rate for I* + RI → RI_2^*

The RI and I* system forms a weakly bound state (-0.07 eV for n-C_3F_7I and -0.04 eV for i-C_3F_7I) through three-body collision (refs. 13 and 32). The exciplex, once formed, decays through emission of 1.3 μm radiation or through transfer of the electronic excitation energy into vibrational-rotational motion of the RI molecule. The overall effect is loss of atomic iodine metastables or quenching of the metastable state. The rate for passing through the exciplex radiative channel is measured by Gerck (ref. 32) to be 6.6×10^{-18} cm^3/sec for n-C_3F_7I and 5.8×10^{-18} cm^3/sec for i-C_3F_7I. Somewhat higher values are observed by Smedley and

Leone (ref. 13) as 10.4×10^{-18} cm^3/sec for n-C_3F_7I and 7.2×10^{-18} cm^3/sec for i-C_3F_7I.

Other Reaction Rates

The remaining reactions in tables V and VI are not expected to contribute, and no reaction rate constants were found in the literature.

SPECTRUM AND GAIN COEFFICIENT OF METASTABLE IODINE

The photodissociation and subsequent chemical reactions govern the production and loss of inversion in the gas. The ability of the gas to amplify a light signal depends on the inversion and stimulated emission cross section. The spectral properties and their relation to the stimulated emission cross section are discussed in this section.

The valance shell of the iodine atom is a $(5p)^5$ configuration with total $L = 1$, $S = 1/2$, and a multiplicity of 2. The ground state is $J = 3/2$ with the first excited state due to spin-orbit interaction $J = 1/2$. In the Russell-Saunders scheme, Garstang (ref. 42) finds a magnetic transition rate of 7.8 sec^{-1} and a small electric quadrupole rate of 0.055 sec^{-1} which yield 0.127 sec as a lifetime of the $^2P_{1/2}$ state, and transition energy of 7605 cm^{-1}. More recent calculations of O'Brien and Bowen (ref. 43) yield 0.11 sec. Experiments were performed by Derwent and Thrush (ref. 44) by which the $^2P_{1/2}$ lifetime was measured relative to the $O_2(^1\Delta)$ lifetime. Assuming the $O_2(^1\Delta)$ lifetime to be 3880 sec yields a lifetime of 0.17 ± 0.04 sec for $^2P_{1/2}$.

Natural iodine occurs as 100-percent I^{127}, for which the nuclear spin is 5/2. The resultant total angular momentum of the whole atom is

$$F = 2,3 \tag{17}$$

for the $^2P_{1/2}$ upper level and

$$F = 1,2,3,4 \tag{18}$$

for the $^2P_{3/2}$ ground state. Because of interaction between the magnetic field of the atomic orbital and the nuclear magnetic moment, the sublevels of different F values are split into distinct lines. In accordance with magnetic selection rules $\Delta F = 0,\pm1$, there are six lines in the $^2P_{1/2} \rightarrow {}^2P_{3/2}$ transition. The energy splitting (ΔE) of the upper levels calculated by Zuev et al. (ref. 45) is

$$\left.\begin{aligned} \Delta E_{F=2} &= -0.371 \text{ cm}^{-1} \\ \Delta E_{F=3} &= 0.265 \text{ cm}^{-1} \end{aligned}\right\} \tag{19}$$

and the splitting of the lower level is

$$\left.\begin{aligned} \Delta E_{F=1} &= -0.118\ \text{cm}^{-1} \\ \Delta E_{F=2} &= -0.094\ \text{cm}^{-1} \\ \Delta E_{F=3} &= -0.028\ \text{cm}^{-1} \\ \Delta E_{F=4} &= 0.113\ \text{cm}^{-1} \end{aligned}\right\} \tag{20}$$

The energy differences between the levels are shown in table VIII along with results of experimental measurements (refs. 45 and 46).

TABLE VIII.- HYPERFINE SPLITTING OF IODINE ^2P STATES

$F_1 - F_2$	$\Delta E_{F_1F_2}$, cm^{-1}					
	$^2P_{1/2}$			$^2P_{3/2}$		
	Theory	Experiment	Ref.	Theory	Experiment	Ref.
1-2				0.025	0.026 ± 0.003 0.025	45 46
2-3	0.636	0.662 ± 0.010 0.69 ± 0.02	45 46	0.0656	0.068 ± 0.002 0.065	45 46
3-4				0.141	0.141 ± 0.002 0.142	45 46

Zuev et al. (ref. 45) calculated the transition rates for the six lines and obtained values shown in table IX. The total lifetime of the upper state was found to be 0.13 sec, which is in good agreement with Garstang (ref. 42).

The hyperfine levels are mixed by thermal collisions in a time which is short compared with its radiative lifetime of 170 msec. The level densities are related by the equilibrium requirement

$$\frac{[I_F^*]}{[I_{F'}^*]} = \frac{g_F}{g_{F'}} \exp\left(-\frac{E_F - E_{F'}}{kT}\right) \tag{21}$$

TABLE IX.- HYPERFINE TRANSITION RATES AND LINE STRENGTHS

Transition	Rate, sec^{-1}	Relative intensity, percent		
		Calculated (this study)	Experiment (ref. 45)	Calculated (ref. 45)
3-4	5.0	37.9	36.5 ± 1.5	37.5
3-3	2.1	16.0	16.3 ± 0.8	16.2
3-2	.6	4.5	6.2 ± 1.1	4.6
2-3	2.4	13.0	13.0 ± 0.6	13.0
2-2	3.0	16.2	15.2 ± 0.7	16.2
2-1	2.3	12.4	12.3 ± 0.5	12.5

where g_F and $g_{F'}$ are the degeneracies, and E_F and $E_{F'}$ are the corresponding energy levels. In equilibrium, the forward and backward reaction rates are likewise equal

$$K_f[I_F^*] = K_b[I_{F'}^*] \tag{22}$$

where K_f and K_b are the forward and backward rate coefficients, respectively, so that

$$K_b = K_f \frac{g_F}{g_{F'}} \exp\left(-\frac{E_F - E_{F'}}{kT}\right) \tag{23}$$

Since the energy separation between the hyperfine sublevels is small compared with the thermal energy, the temperature-dependent factor may be ignored. The ratio of level densities is assumed to be proportional to their degeneracy, the line intensities are calculated, and the corresponding relative intensities for the transition rates are compared with experiments in table IX.

Broadening of Spectral Lines

There are several contributions to the width of a given atomic spectral line. First is the finite lifetime of the level resulting in energy uncertainty at emission. This spectral broadening is impossible to observe under ordinary conditions. There is a Doppler shift due to the relative motion of the atom to the observer. For a gas in thermal equilibrium, the Doppler width is

$$\Delta\nu_D = \frac{2}{c}\left(\frac{kT2\ \ln\ 2}{m}\right)^{1/2} \nu_o$$

$$\Delta\nu_D = 7.162 \times 10^{-7}\ \nu_o\sqrt{T/M} \tag{24}$$

where T is the temperature, and M is the mass of the gas molecule. The relation between the peak of the line shape and the line width is

$$g_o(0) = \frac{2}{\Delta\nu_D}\left(\frac{\ln 2}{\pi}\right)^{1/2} \tag{25}$$

and applies at low gas pressures (ref. 47).

At higher pressures, the interruption of the emission process by binary collisions causes random phase changes in the oscillator frequencies, which further broaden the emission spectrum (ref. 48). The associated line shape is Lorentzian, and the line width is related to the gas collision frequency. Similar to collision broadening is van der Waals broadening, associated with the formation of weakly bound van der Waals molecules. The transition frequency then corresponds to the separation of the two potential curves at the relative nuclear separation at which the transition occurred in accordance with the Franck-Condon principle (ref. 49). The collision and van der Waals broadening are pressure dependent and approximately Lorentzian in profile. The line width is assumed linear in pressure as

$$\Delta\nu = \alpha_1 p \tag{26}$$

where α_1 is the pressure-broadening coefficient. The peak of the line shape is given by

$$g_\ell(0) = \frac{2}{\pi\,\Delta\nu} \tag{27}$$

The line shape function exhibiting the combined effects of the Doppler and Lorentz components is the Voigt function. In the present work, the line shape is approximated by a Lorentzian profile

$$g(\nu) = \frac{\Delta\nu}{2\pi}\,\frac{1}{(\nu - \nu_o)^2 + (\Delta\nu/2)^2} \tag{28}$$

since overlap of the pure Doppler profile of adjacent lines is negligible. The line width is taken as

$$\Delta\nu = \alpha_o + \alpha_1 p \tag{29}$$

where p is the alkyl iodide pressure, and α_o is related to the Doppler line width in equation (24).

Gain and Stimulated Emission Cross Section

The inversion density on a given line is expressed as

$$\Delta I_{FF'} = [I_F^*] - \frac{g_F}{g_{F'}}[I_{F'}] \tag{30}$$

for which the corresponding stimulated emission cross section is

$$\sigma_{FF'}(\nu) = \frac{\lambda^2 A_{FF'}}{8\pi} g_{FF'}(\nu) \tag{31}$$

where $g_{FF'}(\nu)$ is the profile function of the $F \rightarrow F'$ transition, and $A_{FF'}$ is the transition rate. The gain coefficient at a frequency ν is

$$G(\nu) = \sum_{FF'} \sigma_{FF'}(\nu)\ \Delta I_{FF'} \tag{32}$$

which has been studied by several groups. Zuev et al. (ref. 45) measured the line width of the iodine luminescence directly and measured the gain on the 3-4 transition. They conclude that the A_{34} transition rate is $3.4 \pm 1.1\ sec^{-1}$, which implies an Einstein coefficient of

$$A = 5.4 \pm 2\ sec^{-1} \tag{33}$$

in good agreement with the value $6.22 \pm 1.46\ sec^{-1}$ of Derwent and Thrush (ref. 44) but somewhat lower than the $7.86\ sec^{-1}$ of Garstang (ref. 42). The stimulated emission cross section on the 3-4 transition was likewise measured by Fuss and Hohla (ref. 50). The line width was obtained from the measured stimulated emission cross section as

$$\Delta\nu = \frac{A_{34}\lambda^2}{\sigma_{34} 4\pi^2} \tag{34}$$

where they assumed the value of A_{34} to be $5.0\ sec^{-1}$ according to the calculations of Zuev et al. (ref. 45). They obtain for α_1 of equation (29) the value of 20.2 MHz/torr. Baker and King (ref. 51) measure σ_{34} at 100 torr to be $0.9 \pm 0.2 \times 10^{-18}\ cm^2$, which is in good agreement with Zuev et al., who assumed that $A_{34} = 3.4 \pm 1.1\ sec^{-1}$. Nearly perfect agreement between Zuev et al. and Baker and King is obtained for σ_{34} if $A_{34} = 3.7\ sec^{-1}$ is used with the Zuev et al. values.

A detailed study was undertaken by Mukhtar, Baker, and King (ref. 52) in which line width was measured independently of the σ_{34} cross section, and the line-broadening parameter α_1 was found to be 15 ± 4 MHz/torr. Results obtained by Babkin et al. (ref. 53) are quite distinct from the results of references 44, 50, 51, and 52, although the Babkin et al. broadening parameter for CF_3I is in line with Fuss and Hohla (ref. 50). The pressure-broadening parameters of various groups are listed in table X along with estimated temperatures at the time of measurement. The room-temperature parameter is estimated assuming a T dependence. The value adopted here is 14.8 ± 4 MHz/torr.

TABLE X.- PRESSURE-BROADENING PARAMETER FOR C_3F_7I GAS

$\alpha_1(T)$, MHz/torr	T, K	α_1(298 K), MHz/torr	Reference
18 ± 4	530	13.5 ± 3	Zuev et al. (45)
20	420	16.9	Fuss and Hohla (50)
15 ± 4	350	13.9 ± 3.7	Mukhtar et al. (52)
Adopted value		14.8 ± 4	

EFFECTS OF DIFFUSION

Diffusion of the iodine metastable within the laser tube with finite dimension is an additional process by which inversion is lost within the gas. The diffusion proceeds in two steps associated with thermalization of the hot photodissociation products followed by slow thermal diffusion.

The iodine metastable is produced with kinetic energy of 0.79 eV and undergoes 4 to 5 collisions before thermalization takes place. The distance traveled in thermalization is

$$d \sim 0.5 \text{ mm-torr} \tag{35}$$

which is small compared with the radius of the laser tube (≈3.5 mm) even at 1 torr. However, the thermal diffusion may be quite important. Considering the expected high sticking factor of the iodine atom at the quartz wall (ref. 54), such collisions appear as a loss of excitation energy from the inversion density.

The particles produced at an instant in time at the origin of a coordinate frame as a result of gaseous diffusion are distributed in space at a later time t according to

$$n_{I^*}(r,t) = \frac{2n_o}{\pi(4Dt)^{3/2}} \exp\left(\frac{-r^2}{4Dt}\right) \tag{36}$$

where n_o is the initial density of metastables, r is the distance from the origin, and D is the diffusion coefficient (ref. 55). In the laser, the source of I* is relatively uniform over several millimeters, so that losses due to diffusion from one point are compensated by diffusion from adjacent source points. Only by diffusion to the glass surface are particles lost. Density changes on the tube axis are then proportional to

$$n_{I^*}(0,t) = \frac{2n_o}{\pi} \int_{-\infty}^{\infty} d\ell \int_0^{r_o} r\, dr\, \frac{1}{(4Dt)^{3/2}} \exp\left[\frac{-(r^2 + \ell^2)}{4Dt}\right]$$

$$n_{I^*}(0,t) = n_o\left[1 - \exp\left(\frac{-r_o^2}{4Dt}\right)\right] \tag{37}$$

where r_o is the inside radius of the laser tube. A diffusion time constant can be defined by using equation (37) as

$$\tau_D \approx \frac{r_o^2}{2D} \tag{38}$$

where τ_D is the mean diffusion time from the centerline to the tube wall.

The diffusion coefficient for isotropic scattering is related to the elastic scattering mean free path λ_s as

$$D = \frac{1}{2}\lambda_s v \tag{39}$$

where v is the mean thermal speed of the diffusing particle. The iodine atomic radius is 215 pm (ref. 9), the alkyl iodide radius is estimated from binary diffusion (ref. 56) to be 400 pm, and the mean thermal velocity of the iodine atom is 1.92×10^4 cm/sec (298 K). Using the iodine atomic radius and the alkyl iodide radius yields 3.8×10^{-15} cm^2 for the scattering cross section and 0.0076 cm-torr for mean free path so that equation (39) yields

$$D \approx 73 \text{ cm}^2\text{-torr/sec} \tag{40}$$

The laser tube radius of 3.5 mm yields a diffusion lifetime of

$$\tau_D \approx 8.5 \times 10^{-4} \text{ sec/torr} \tag{41}$$

for the present experiments.

PHOTOLYSIS OF ALKYL IODIDES

The chemical and physical processes being outlined in previous sections, a mathematical model describing the rate of change of specific densities of constituents in the laser tube is described in this section. The major kinetic pathways are first summarized. The initial excitation of the gas is through photodissociation into excited iodine and the C_3F_7 radical denoted by the zigzag line in figure 7. The loss of excited iodine through radiative decay is slow (see zigzag line between I* and I in fig. 7), so that excited iodine loss is mainly through the slow recombination

$$R + I^* \rightarrow RI$$

which allows large metastable populations. Further losses of excited iodine occur through collisional quenching, especially if contamination of the gas with I_2, H_2O, or O_2 occurs. The ground-state iodine rapidly combines with the free radical C_3F_7. This recombination is necessary for maintaining the inversion. More slowly, the ground-state iodine recombines with either ground-state iodine or metastable iodine to form iodine molecules. Due to the presence of intense visible radiation, the iodine molecule photodissociates to form ground-state and metastable iodine.

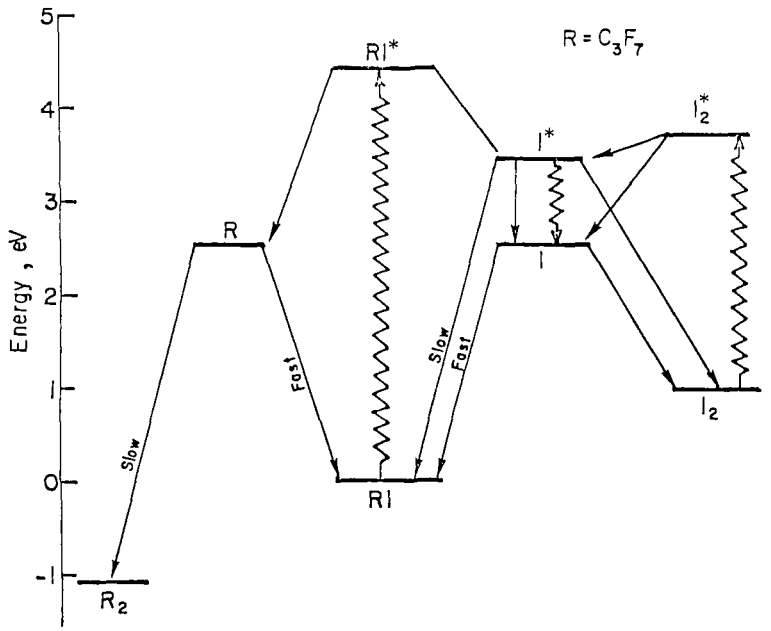

Figure 7.- Major kinetic pathways of the iodine laser.

The major kinetic pathways are summarized in figure 7. The photodissociation rates are given by equation (15), where the parameters are those in table II. The maximum gain will occur on the tube centerline on which the kinetic equations are to be solved. Diffusion effects are ignored except for diffusion of the iodine atoms to the inner wall, where they are assumed to have a sticking factor of unity (ref. 54).

The RI molecule photodissociates at a rate ξ_1 to form R and I*. The hot radical R is assumed to collide with the RI molecule to form dimer R_2 and ground-state iodine with rate coefficient K_4. The RI is reformed by recombination with I or I* as depicted in

$$\frac{d[RI]}{dt} = K_1[R][I^*] + K_2[R][I] - K_4[R][RI] - \xi_1 \tag{42}$$

where brackets around a chemical species denote its density. Note, this is an approximate representation for hot radical reaction. The source of the free radical R is photodissociation of RI. Losses occur through recombination of R with R, I, or I*. Additional loss occurs through hot radical reaction

$$\frac{d[R]}{dt} = \xi_1 - K_1[R][I^*] - K_2[R][I] - 2K_3[R]^2 - K_4[RI][R] \tag{43}$$

The dimer is formed by radical recombination or hot radical reaction

$$\frac{d[R_2]}{dt} = K_3[R]^2 + K_4[R][RI] \tag{44}$$

The iodine molecule is formed through three-body recombination of iodine atoms and metastables. The metastables do not recombine because of mutual repulsion. The iodine molecules are lost through photodissociation. The rate of change of iodine molecules is given by

$$\frac{d[I_2]}{dt} = C_1[I][I^*][RI] + C_2[I]^2[RI] + C_3[I][I^*][I_2] + C_4[I]^2[I_2] - \xi_2 \tag{45}$$

The iodine metastable is formed through photodissociation of RI and I_2. It is lost mainly through recombination with R. Slower loss processes include three-body recombination with iodine atoms and quenching with RI and I_2 molecules. Further loss occurs through radiative decay and diffusion to the cell wall. The resultant rate equation for metastable density is

$$\frac{d[I^*]}{dt} = \xi_1 + \xi_2 - K_1[R][I^*] - C_1[I][I^*][RI] - C_3[I][I^*][I_2]$$

$$- Q_1[I^*][RI] - Q_2[I^*][I_2] - A[I^*] - \frac{[I^*]}{\tau_D} \tag{46}$$

Ground-state iodine atoms are produced through photodissociation of I_2, quenching, and radiative decay of iodine metastable. A small source is hot radical reaction with RI. Losses are mainly through R + I recombination, and smaller losses appear through three-body recombination and diffusion to the cell wall. The total atomic iodine change in time is given by

$$\frac{d[I]}{dt} = \xi_2[I_2] + Q_1[I^*][RI] + Q_2[I^*][I_2] + K_4[R][RI]$$

$$+ A[I^*] - C_1[I][I^*][RI] - 2C_2[I]^2[RI] - C_3[I][I^*][I_2]$$

$$- 2C_4[I]^2[I_2] - K_2[R][I] - \frac{[I]}{\tau_D} \qquad (47)$$

Equations (42) through (47) apply at any location on the laser centerline if no longitudinal diffusion is assumed. Kinetic rate coefficients are given in table VII.

Consider the initial illumination of the lasant gas, for which all other constituent densities are initially zero. The most important processes are

$$RI + h\nu \rightarrow R + I^*$$

$$R + I^* \rightarrow RI$$

and to a lesser extent

$$I^* + RI \rightarrow I + RI$$

and diffusion at low pressures. To a good approximation, the R and I* densities are equal, so equation (46) becomes

$$\frac{d[I^*]}{dt} = \xi_1 - K_1[I^*]^2 - Q_1[RI][I^*] - \frac{[I^*]}{\tau_D} \qquad (48)$$

the solution of which is given by

$$[I^*] = \frac{A^2 - \tau^{-2}}{2K_1} \frac{1 - \exp(-At)}{A + \tau^{-1} + (A - \tau^{-1}) \exp(-At)} \qquad (49)$$

where

$$A = \sqrt{4\xi_1 K_1 + \tau^{-2}} \tag{50}$$

and

$$\tau^{-1} = Q_1[RI] + \tau_D^{-1} \tag{51}$$

It is clear that the inversion density is closely related to the rate coefficients K_1 and Q_1 and to the diffusion constant τ_D.

The time constant associated with reaching steady state is found from equation (50) to be

$$A^{-1} \approx \frac{100}{\sqrt{pC}} \text{ (msec)} \tag{52}$$

where C is the solar concentration, and p is the alkyl iodide pressure in torr. In actual practice, the light input is modulated by a chopper for which the rise time is on the order of a few milliseconds. (See fig. 8.) The effective time constant is then extended from the value in equation (52) by the amount

$$A^{-1} \approx \frac{100}{\sqrt{pC\ f(t)}} \tag{53}$$

where $f(t)$ is the light modulation function, which is initially zero and which rises to unity in ≈2.5 msec. The solution is more accurately given by

$$[I^*] \approx \frac{A - \tau^{-1}}{2K_1} \frac{1 - \exp(-At/3)}{1 + \exp(-3At)} \tag{54}$$

where A is time dependent according to equation (53).

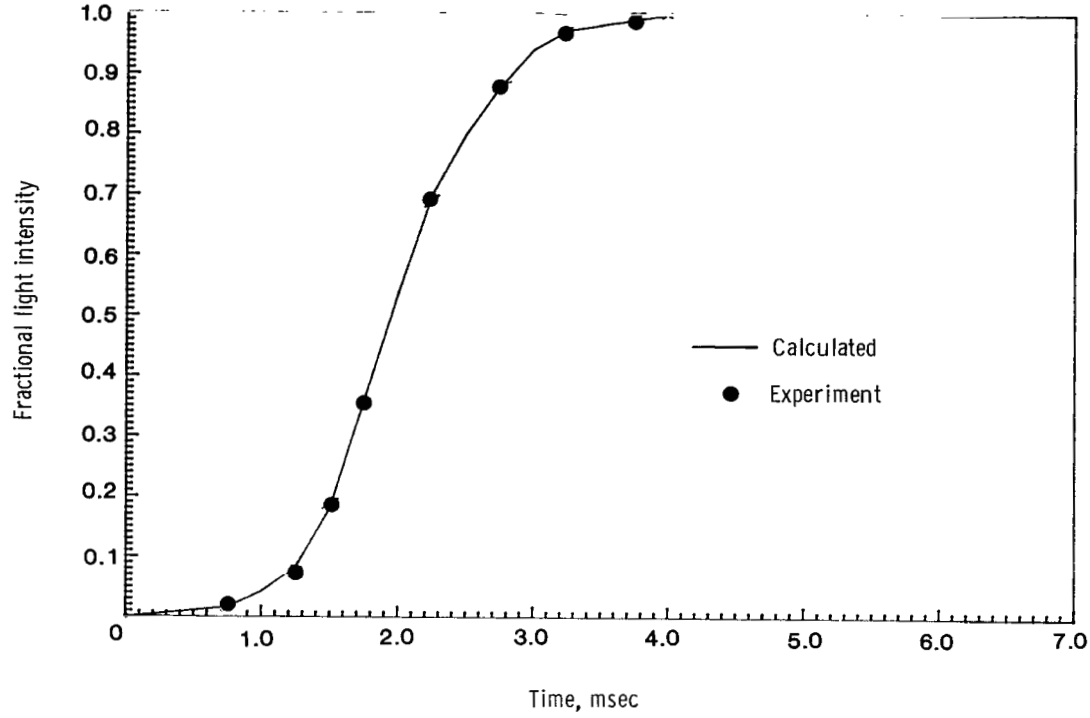

Figure 8.- Light intensity modulation function used in model compared with light measurements for chopper used in experiments.

In most cases of interest, threshold is reached in a fraction of a millisecond, for which equation (54) is far from its steady-state value, so that expansion of equation (54) for small values of At yields

$$[I^*] \approx \xi_1 \frac{t^2}{3t_c} \tag{55}$$

as one would expect on observing equation (48). In equation (55), t_c is the rise time of the chopper modulation function ($t_c \approx 2$ msec). The relation of the I* density to the pump source yields the spatial dependence of the inversion density for which the average gain over the tube length may be found.

MAXIMUM GAIN

The equations of photolysis are integrated numerically at the most intense position of the light source. The pump light is modulated by the mechanical chopper according to a modulation function which rises in 2.5 msec, holds near unity for 4 msec, and declines over the next 2.5 msec. The maximum gain occurs on the 3-4 transition because of the high population in the F = 3 upper level (eq. (21)) and the high transition rate to the F = 4 lower level (table IX). In accordance

with the definitions of Fuss and Hohla (ref. 50), the gain coefficient for the 3-4 transition is taken as

$$G_{34} = \sum_{FF'} \sigma_{FF'}(\nu_{34})\ \Delta I_{FF'}$$

$$G_{34} \approx \left[\sum_{FF'} \sigma_{FF'}(\nu_{34})\right] \frac{g_3}{g_2 + g_3}\ \Delta I \tag{56}$$

where the total population inversion between $P_{1/2}$ and $P_{3/2}$ is

$$\Delta I = [I^*] - \frac{[I]}{2} \tag{57}$$

and the ratio $g_3/(g_2 + g_3)$ is the approximate fraction of the inversion which contributes to the 3-4 transition (ref. 50). The stimulated emission cross section is then taken as

$$\sigma^*_{34} = \frac{g_3}{g_2 + g_3} \sum_{FF'} \sigma_{FF'}(\nu_{34}) \tag{58}$$

The individual values of $\sigma_{FF'}(\nu_{34})$ are evaluated using equation (31). The inversion varies along the axis of the tube in approximate proportion to the illumination by the arc image. (See eqs. (4) and (55).) The total round-trip amplification of the gas on the axis of the tube is then

$$G' = \exp\left[2 \int_{-\infty}^{\infty} G_{34} \exp\left(\frac{-2.77\ell^2}{L^2}\right) d\ell\right]$$

$$G' = \exp\left(2\sqrt{\frac{\pi}{2.77}}\ L\sigma^*_{34}\ \Delta I\right) \tag{59}$$

which must balance the losses at the tube windows and end mirrors (with effective reflectances R_1 and R_2) as

$$R_1 R_2 \exp\left(2\sqrt{\frac{\pi}{2.77}}\ L\sigma^*_{34}\ \Delta I\right) = 1 \tag{60}$$

The inversion density ΔI depends mainly on the kinetic coefficients K_1 and Q_1 and the diffusion coefficient for I* in RI as seen in equations (49) to (51). The stimulated emission cross section depends on the pressure-broadening coefficient α_1. These parameters will now be investigated from the point of view of threshold measurements on solar-simulator-pumped lasers.

COMPARISON WITH EXPERIMENTAL RESULTS

Threshold was investigated experimentally with the setup depicted in figure 1. Before each experimental run, the laser tube was evacuated to $\approx 10^{-6}$ torr and filled with purified lasant gas ($n\text{-}C_3F_7I$) through a copper gas-handling system. Prior to use in experiments, the lasant was purified by distillation. Because of the temporal oscillations of the arc light source, many experimental runs were generally made at each fill pressure in an attempt to identify ideal exposure conditions. The identification of maximum pump rate was made by placing threshold measurements at each pressure into a sequence of decreasing values, which should provide a sequence which approaches the model from above. Threshold was identified by the beginning of the first laser pulse and recorded as the fraction of the peak light intensity of the solar-simulator output pulse. Note that the threshold condition expressed in this way depends on the chopper geometry and speed, since threshold is achieved before the photolysis establishes equilibrium with the solar-simulator light source. Before an attempt to compare the model with the experiments was made, the sensitivity of threshold to the coefficients K_1, Q_1, and α_1 was determined. First, the kinetic equations were integrated numerically by using the mean values of all coefficients shown in table VII. The threshold as a function of pressure for the mean values of parameters is shown in figure 9 as the lower curve. Then each of the

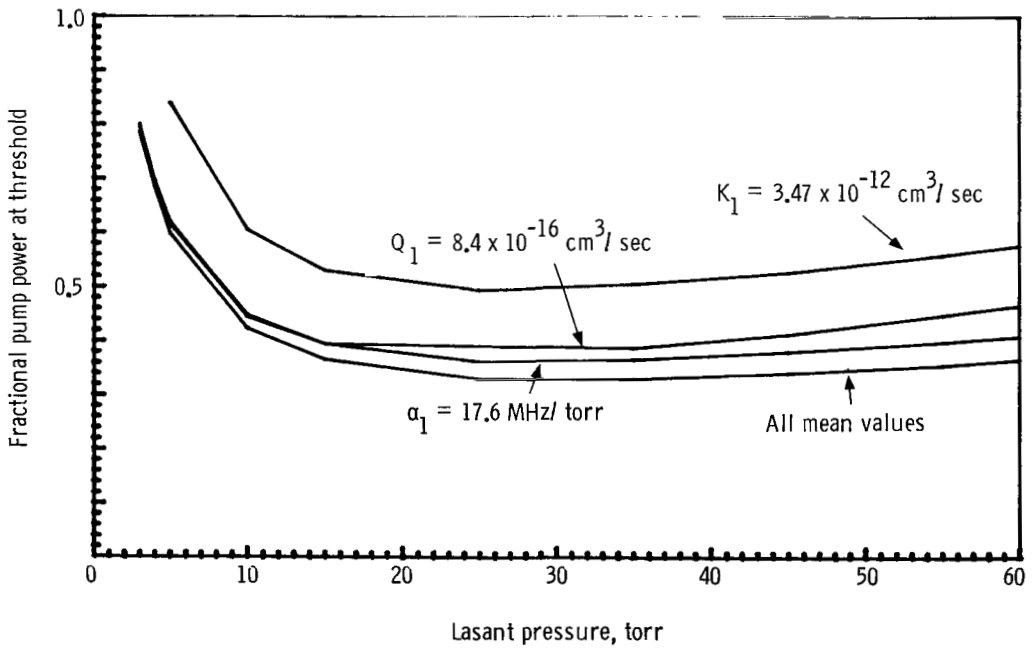

Figure 9.- Mean threshold and threshold sensitivity to experimental uncertainty in specific rate coefficients and pressure broadening.

parameters K_1, Q_1, and α_1 was allowed to take its maximum value specified in table VII one at a time to determine the sensitivity of threshold to each. These results are shown in figure 9. It is seen that K_1 affects the threshold almost equally at all pressures. Q_1 causes little effect below 5 torr but a very large effect at 60 torr. The pressure-broadening coefficient α_1 shows a slight effect at low pressure and greater effect with increasing pressure. Parameters were so chosen as to provide the most reasonable agreement with experiments from the three conic collectors. Results are shown in figures 10, 11, and 12. The calibration shown in figure 2 for the cone with a 23.6-cm-diameter aperture results in $C_o\sqrt{L} = 618$, which compares with a more recent calibration on July 31, 1981, which yielded $C_o\sqrt{L} \approx 540$. The results shown in figure 12 are calculated for the July 31, 1981, calibration. The final values used were

$$K_1 = 2.0 \times 10^{-12} \text{ cm}^3/\text{sec}$$

$$Q_1 = 8.4 \times 10^{-16} \text{ cm}^3/\text{sec}$$

$$\alpha_1 = 17.6 \text{ MHz/torr}$$

It is noted that Q_1 and α_1 are similar in their effect on threshold. The high values of Q_1 used here may be caused by gas impurity. These results are summarized in table XI along with results of the previous analysis of the solar-simulator-pumped iodine laser experiments (ref. 4).

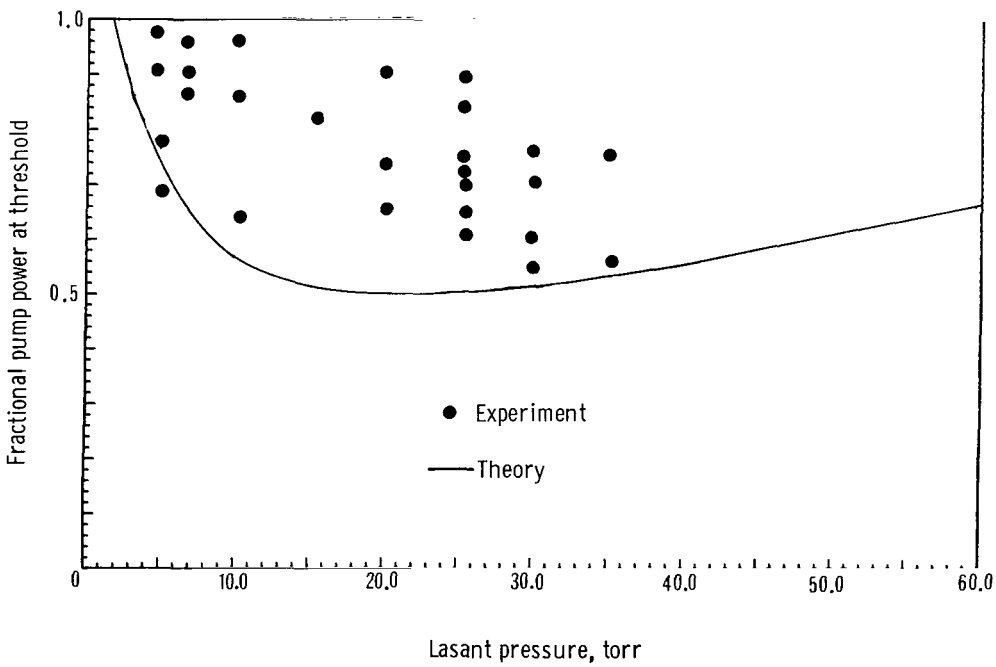

Figure 10.- Comparison between theoretical and experimental threshold for cone with 9.6-cm-diameter aperture.

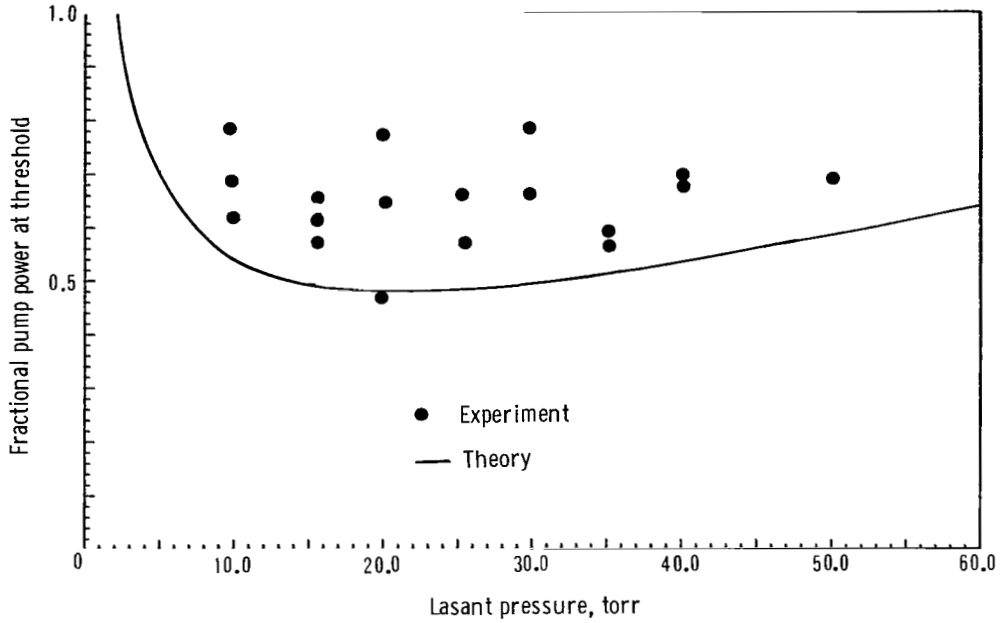

Figure 11.- Comparison between theoretical and experimental threshold for cone with 16.6-cm-diameter aperture.

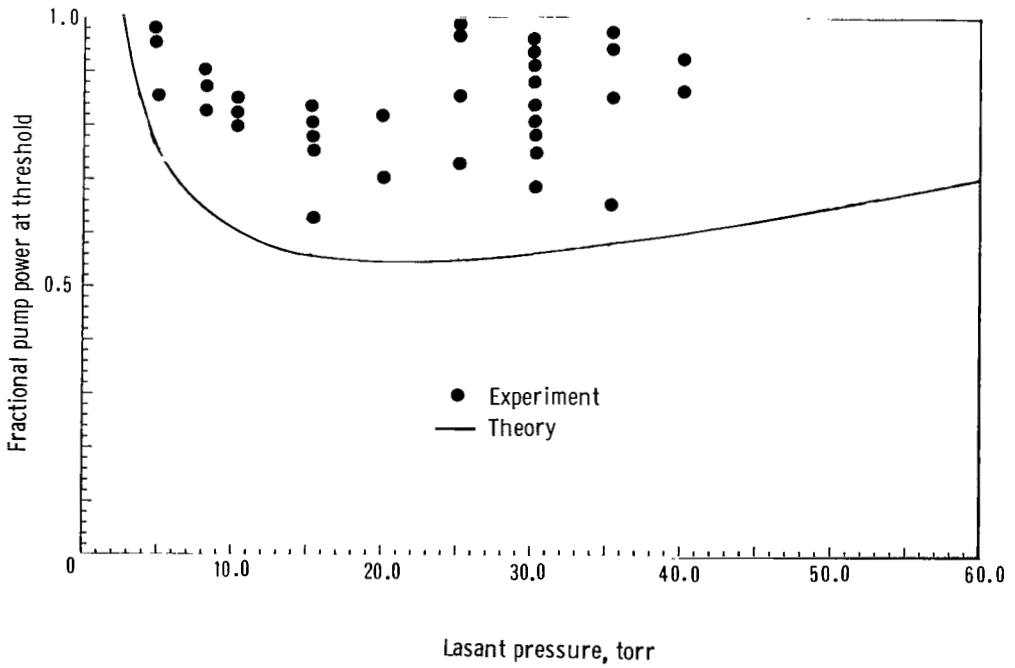

Figure 12.- Comparison between theoretical and experimental threshold for cone with 23.6-cm-diameter aperture.

TABLE XI.- IODINE LASER KINETIC RATE COEFFICIENTS ACCORDING TO ANALYSIS OF SOLAR-SIMULATOR EXPERIMENTS WITH $n\text{-}C_3F_7I$

[The factor in parentheses gives the uncertainty limits associated with the coefficient]

Coefficient	From table VII or X	Solar simulator
K_1, cm^3/sec	5.6×10^{-13} $(6.2)^{\pm 1}$	2.0×10^{-12}
K_2, cm^3/sec	2.3×10^{-11} $(3.5)^{\pm 1}$	4.3×10^{-11} $(1.9)^{\pm 1}$
K_3, cm^3/sec	2.6×10^{-12} $(4)^{\pm 1}$	
K_4, cm^3/sec	3×10^{-16}	
Q_1, cm^3/sec	2.0×10^{-16} $(4.2)^{\pm 1}$	8.4×10^{-16}
Q_2, cm^3/sec	1.9×10^{-11} $(2.6)^{\pm 1}$	3.1×10^{-11} $(1.6)^{\pm 1}$
C_1, cm^6/sec	3.2×10^{-33} $(3.2)^{\pm 1}$	
C_2, cm^6/sec	8.5×10^{-32} $(5.3)^{\pm 1}$	3.7×10^{-32} $(2.3)^{\pm 1}$
C_3, cm^6/sec	8×10^{-32} $(1.8)^{\pm 1}$	
C_4, cm^6/sec	3.8×10^{-30} $(1.3)^{\pm 1}$	
α_1, MHz/torr	14.8 ± 4	17.6

CONCLUDING REMARKS

A detailed model of the chemical kinetics of the $n\text{-}C_3F_7I$ solar-simulator-pumped iodine laser is utilized to study the major kinetic processes associated with the threshold behavior of this experimental system. Excited-state diffusion to the cell wall is the dominant limiting factor below 5 torr. Excited-state recombination with the alkyl radical (R) and quenching by the parent gas control threshold at higher pressures. Treatment of the hyperfine splitting and uncertainty in the pressure broadening are important factors in fixing the threshold level.

The trends of the experimental threshold measurements are well represented by the present model. Even the scaling with respect to peak light input intensity and gain length for the three conic collectors is quite consistent. The final value of the recombination rate for

$$I^* + R \rightarrow RI$$

is on the high side of the results reported by most other workers. Compared with values for $i\text{-}C_3F_7$ recombination, our value is slightly smaller than the recent value

of Ershov et al. (Soviet J. Quantum Electron., vol. 8, no. 4, 1978) but 3 times larger than Skorobogatov and Slesar (Vestn. Leningr. Univ. Fiz. Khim., vol. 4, no. 1, 1979). The metastable quenching rate is quite high and may be indicative of contamination of the parent gas. The final value of the pressure-broadening coefficient is large compared with others. There is some dependence of pressure broadening and quenching coefficient so they can, to some degree, be traded off without affecting threshold in the model. If the gas is sufficiently contaminated, then pressure broadening may be less than indicated.

The present compilation of data indicates that the isopropyl form of the alkyl iodide should have a lower threshold because of the larger photodissociation rates and slower recombination and quenching rates. It would be interesting to make such a comparison. Finally, experiments in which better control over experimental light input and gas contamination effects would be useful in resolving disagreement among various experimenters on the recombination and quenching rates.

Langley Research Center
National Aeronautics and Space Administration
Hampton, VA 23665
December 12, 1983

REFERENCES

1. Rather, John D. G.: New Candidate Lasers for Power Beaming and Discussion of Their Applications. Radiation Energy Conversion in Space, Kenneth W. Billman, ed., AIAA, c.1978, pp. 313-332.

2. Lee, Ja H.; and Weaver, W. R.: A Solar Simulator-Pumped Atomic Iodine Laser. Appl. Phys. Lett., vol. 39, no. 2, July 15, 1981, pp. 137-139.

3. Wilson, J. W.; and Lee, J. H.: Modeling of a Solar-Pumped Iodine Laser. Virginia J. Sci., vol. 31, no. 3, Fall 1980, pp. 34-38.

4. Wilson, John W.; Raju, S.; and Shiu, Y. J.: Solar-Simulator-Pumped Atomic Iodine Laser Kinetics. NASA TP-2182, 1983.

5. Koffend, J. Brooke; and Leone, Stephen R.: Tunable Laser Photodissociation: Quantum Yield of I* ($^2P_{1/2}$) From CH_2I_2. Chem. Phys. Lett., vol. 81, no. 1, July 1, 1981, pp. 136-141.

6. Leone, Stephen R.: Molecular Photofragmentation Processes Related to Solar-Pumped Gas Laser Development. NASA CR-169408, 1982.

7. Wilson, Kent R.: Photofragment Spectroscopy of Dissociative Excited States. Excited State Chemistry, James N. Pitts, ed., Gordon & Breach, Science Pub., Inc., c.1970, pp. 33-58.

8. Krylov, Vladimir Ivanovich (Arthur H. Stroud, transl.): Approximate Calculation of Integrals. Macmillan Co., c.1962.

9. Huheey, James E.: Inorganic Chemistry: Principles of Structure and Reactivity, Second ed. Harper & Row, 1978.

10. Silverstein, Robert M.; Bassler, G. Clayton; and Morrill, Terence C.: Spectrometric Identification of Organic Compounds, Fourth ed. John Wiley & Sons, Inc., c.1981.

11. Butler, Ronald L.; and Snelson, A.: IR Matrix Isolation Product Characterization From Low-Pressure Pyrolysis of $C_nF_{2n+1}I$ (n = 1-4) and C_6F_5I. J. Fluorine Chem., vol. 15, no. 4, 1980, pp. 345-349.

12. Badger, Richard M.: The Relation Between the Internuclear Distance and Force Constants of Molecules and Its Application to Polyatomic Molecules. J. Chem. Phys., vol. 3, no. 11, Nov. 1935, pp. 710-714.

13. Smedley, John E.; and Leone, Stephen R.: Relative Quantum Yield of I*($^2P_{1/2}$) in the Tunable Laser UV Photodissociation of i-C_3F_7I and n-C_3F_7I: Effect of Temperature and Exciplex Emission. J. Chem. Phys., vol. 79, no. 6, Sept. 15, 1983, pp. 2687-2695.

14. Hohla, K.; and Kompa, K. L.: Kinetische Prozesse in Einem Photochemischen Jodlaser. Z. Naturforsch., vol. 27a, no. 6, June 1972, pp. 938-947.

15. Turner, C. E., Jr.; and Rapagnani, N. L.: Kinetic Modeling of Photodissociation Iodine Laser Amplifiers. UCID-16935 (Contract No. W-7405-Eng-48), Lawrence Livermore Lab., Univ. of California, Oct. 23, 1974.

16. Kuznetsova, S. V.; and Maslov, A. I.: Investigation of the Reactions of Atomic Iodine in Photodissociation Laser Using n-C_3F_7I and i-C_3F_7I Molecules. Soviet J. Quantum Electron., vol. 3, no. 6, May-June 1974, pp. 468-471.

17. Beverly, R. E., III; and Wong, M. C.: Transverse-Discharge Excitation of the 1.315-μm Atomic Iodine Laser. II. Kinetic Model. Opt. Commun., vol. 20, no. 1, Jan. 1977, pp. 23-28.

18. Fisk, George A.: The Effects of Chemical Kinetics and Starting Material Regeneration on the Efficiency of an Iodine Laser Amplifier. Rep. SAND77-0880, Sandia Labs., May 1977.

19. Kuznetsova, S. V.; and Maslov, A. I.: New Reaction Rate Constants of CF_3, n-C_3F_7, and i-C_3F_7 Radicals. Soviet J. Quantum Electron., vol. 8, no. 7, July 1978, pp. 906-909.

20. Skorobogatov, G. A.; and Slesar, O. N.: Measurement of the Absolute Rate Constants of the Gas-Phase Recombination Reactions of Fluorocarbon Radicals With Themselves and With Iodine Atoms. Vestn. Leningr. Univ. Fiz. Khim., vol. 4, no. 1, 1979, pp. 39-45.

21. Skorobogatov, G. A.; Komarov, V. S.; and Seleznev, V. G.: Absolute-Photometry Determination of the Rate Constant of the Gas-Phase Reaction of the Radical Compound C_3F_7 and $I(^2P_{3/2})$. Soviet Phys. - Tech. Phys., vol. 19, no. 9, Mar. 1975, pp. 1239-1241.

22. Zalesskii, V. Yu.; and Venediktov, A. A.: Mechanism of Generation and Termination at the $5^2P_{1/2}$-$5^2P_{3/2}$ Transition in Iodine. Soviet Phys. - JETP, vol 28, no. 6, June 1969, pp. 1104-1107.

23. Christie, Margaret I.; Harrison, Anna J.; Norrish, R. G. W.; and Porter, G.: The Recombination of Atoms. II. Causes of Variation in the Observed Rate Constant for Iodine Atoms. Proc. R. Soc. London, ser. A, vol. 231, no. 118, Sept. 20, 1955, pp. 446-457.

24. Ershov, L. S.; Zalesskii, V. Yu.; and Kokushkin, A. N.: Determination of the Rate Constants for Iodine Atom Recombination in the Presence of Perfluoroalkyl Iodides. High Energy Chem., vol. 8, no. 3, Nov. 1974, pp. 188-190.

25. Bunker, Don L.; and Davidson, Norman: A Further Study of the Flash Photolysis of Iodine. J. American Chem. Soc., vol. 80, no. 19, Oct. 5, 1958, pp. 5085-5090.

26. Blake, J. A.; and Burns, George: Kinetics of Iodine Atom Recombination Between 300° and 1164°K. J. Chem. Phys., vol. 54, no. 4, Feb. 15, 1971, pp. 1480-1486.

27. Busch, George E.: Kinetic Analyses of Energy Storage in a Chemically Pumped Iodine Laser. IEEE J. Quantum Electron., vol. QE-17, no. 6, June 1981, pp. 1128-1133.

28. Andreeva, T. L.; Kuznetsova, S. V.; Maslov, A. I.; Sobel'man, I. I.; and Sorokin, V. N.: Investigation of Reactions of Excited Iodine Atoms With the Aid of a Photodissociation Laser. J. Exp. & Theor. Phys. Lett., vol. 13, no. 11, June 5, 1971, pp. 449-452.

29. Ershov, L. S.; Zalesskii, V. Yu.; and Sokolov, V. N.: Laser Photolysis of Perfluoroalkyl Iodides. Soviet J. Quantum Electron., vol. 8, no. 4, Apr. 1978, pp. 494-501.

30. Vinokurov, G. N.; and Zalesskii, V. Yu.: Chemical Kinetics and Gasdynamics of a Q-Switched Iodine Laser With an Optically Thick Active Medium. Soviet J. Quantum Electron., vol. 8, no. 10, Oct. 1978, pp. 1191-1197.

31. Wilson, John W.: Solar-Pumped Gas Laser Development. NASA TM-81894, 1980.

32. Gerck, Edgardo: Collisional Enhancement of the $I(5^2P_{1/2})$ Emission at 1.3 μm by Parent Molecules CF_3I, C_2F_5I, $i\text{-}C_3F_7I$ and $n\text{-}C_3F_7I$. Opt. Commun., vol. 41, no. 2, Mar. 15, 1982, pp. 102-105.

33. Stephan, K.-H.; and Comes, F. J.: Chemiluminescent Iodine Atom Recombination. Chem. Phys. Lett., vol. 65, no. 2, Aug. 15, 1979, pp. 251-256.

34. Comes, F. J.; and Pionteck, S.: UV Photolysis of $n\text{-}C_3F_7I$. Radiative Lifetime of Metastable Iodine Atoms. Chem. Phys. Lett., vol. 58, no. 4, Oct. 15, 1978, pp. 616-618.

35. Dobychin, S. L.; Mikheev, L. D.; Pavlov, A. B.; Fokanov, V. P.; and Khodarkovskii, M. A.: Quenching of Excited Iodine Atoms $I(5^2P_{1/2})$ by Molecules With C-I Bonds. Soviet J. Quantum Electron., vol. 8, no. 11, Nov. 1978, pp. 1383-1384.

36. Hofmann, Hubert; and Leone, Stephen R.: Collisional Deactivation of Laser-Excited Br* ($^2P_{1/2}$) Atoms With Halogen and Interhalogen Molecules. Chem. Phys. Lett., vol. 54, no. 2, Mar. 1, 1978, pp. 314-319.

37. Donovan, R. J.; and Husain, D.: Spin Orbit Relaxation of Metastable Iodine Atoms. Nature, vol. 206, no. 4980, Apr. 10, 1965, pp. 171-173.

38. Kartazaev, V. A.; Penkin, N. P.; and Tolmachev, Yu. A.: Determination of the Temperature Dependence of the Rate Constant Representing Quenching of Metastable Iodine Atoms by Iodine Molecules. Soviet J. Quantum Electron., vol. 7, no. 5, May 1977, pp. 608-610.

39. Arnold, I.; Comes, F. J.; and Pionteck, S.: Laser Induced Photodissociation of Iodine Molecules. Spin-Orbit Relaxation of $I(^2P_{1/2})$. Chem. Phys., vol. 9, nos. 1,2, June 1975, pp. 237-240.

40. Andreeva, T. L.; Malyshev, V. I.; Maslov, A. I.; Sobel'man, I. I.; and Sorokin, V. N.: Possibility of Obtaining Excited Iodine Ions as a Result of Chemical Reactions. J. Exp. & Theor. Phys. Lett., vol. 10, no. 9, Nov. 5, 1969, pp. 271-274.

41. Zalesskii, V. Yu.; and Krupenikova, T. I.: Deactivation of Metastable Iodine Atoms by Collision With Perfluoroalkyliodide Molecules. Opt. & Spectry. (USSR), vol. 30, no. 5, May 1971, pp. 439-443.

42. Garstang, R. H.: Transition Probabilities of Forbidden Lines. J. Res. Nat. Bur. Stand., vol. 68A, no. 1, Jan.-Feb. 1964, pp. 61-73.

43. O'Brien, Dennis E.; and Bowen, J. Ray: Kinetic Model for the Iodine Photodissociation Laser. J. Appl. Phys., vol. 40, no. 12, Nov. 1969, pp. 4767-4769.

44. Derwent, R. G.; and Thrush, B. A.: The Radiative Lifetime of the Metastable Iodine Atom $I(5^2P_{1/2})$. Chem. Phys. Lett., vol. 9, no. 6, June 15, 1971, pp. 591-592.

45. Zuev, V. S.; Katulin, V. A.; Nosach, V. Yu.; and Nosach, O. Yu.: Investigation of the Luminescence Spectrum of Atomic Iodine ($^2P_{1/2}$-$^2P_{3/2}$ Laser Transition. Soviet Phys. - JETP, vol. 35, no. 5, Nov. 1972, pp. 870-873.

46. Hwang, W. C.; and Kasper, J. V. V.: Zeeman Effects in the Hyperfine Structure of Atomic Iodine Photodissociation Laser Emission. Chem. Phys. Lett., vol. 13, no. 5, Apr. 1, 1972, pp. 511-514.

47. Lengyel, Bela A.: Introduction to Laser Physics. John Wiley & Sons, Inc., c.1966.

48. Siegman, A. E.: An Introduction to Lasers and Masers. McGraw-Hill, Inc., c.1971, chapter 3.

49. Herzberg, Gerhard: Molecular Spectra and Molecular Structure. I. Spectra of Diatomic Molecules, Second ed. D. Van Nostrand Co., Inc., c.1950, chapter VII.

50. Fuss, W.; and Hohla, K. (D. K. Dreyer and R. E. Beverly III, transl.): Pressure Broadening of the 1.3 μm Iodine Laser Line. Rep. No. IPP IV/67, Max-Planck-Inst. für Plasmaphysik (Garching bei München), Dec. 1974. Also, Fuss, W.; and Hohla, K.: Pressure Broadening of the 1.3 μm Iodine Laser Line. Z. Naturforsch., vol. 31a, no. 6, June 1976, pp. 569-577.

51. Baker, H. J.; and King, T. A.: Iodine Photodissociation Laser Oscillator Characteristics. J. Phys. D: Appl. Phys., vol. 8, no. 6, Apr. 21, 1975, pp. 609-619.

52. Mukhtar, E. S.; Baker, H. J.; and King, T. A.: Hyperfine Structure and Collision Parameters of the 1.315 μm Iodine Laser Transition Studied by a Frequency-Controlled Laser. J. Phys. D: Appl. Phys., vol. 11, no. 9, June 21, 1978, pp. 1303-1318.

53. Babkin, V. I.; Kuznetsova, S. V.; and Maslov, A. I.: Simple Method for Determination of Stimulated Emission Cross Section of $^2P_{1/2}(F=3) \rightarrow {}^2P_{3/2}(F'=4)$ Transition in Atomic Iodine. Soviet J. Quantum Electron., vol. 8, no. 3, Mar. 1978, pp. 285-289.

54. Young, D. M.; and Crowell, A. D.: Physical Adsorption of Gases. Butterworths, 1962.

55. Liverhant, S. E.: Nuclear Reactor Physics. John Wiley & Sons, Inc., c.1960, p. 246.

56. Belousova, I. M.; Kiselev, V. M.; and Kurzenkov, V. N.: Diffusion of CF_3I and C_3F_7I in Inert Gases. Soviet Phys. - Tech. Phys., vol. 15, no. 2, Aug. 1970, pp. 301-302.

1. Report No.	2. Government Accession No.	3. Recipient's Catalog No.
NASA TP-2241		

4. Title and Subtitle	5. Report Date
THRESHOLD KINETICS OF A SOLAR-SIMULATOR-PUMPED IODINE LASER	February 1984
	6. Performing Organization Code 506-55-13-01
7. Author(s)	8. Performing Organization Report No.
John W. Wilson, Yeunggil Lee, Willard R. Weaver, Donald H. Humes, and Ja H. Lee	L-15684
	10. Work Unit No.
9. Performing Organization Name and Address	11. Contract or Grant No.
NASA Langley Research Center Hampton, VA 23665	
	13. Type of Report and Period Covered
12. Sponsoring Agency Name and Address	Technical Paper
National Aeronautics and Space Administration Washington, DC 20546	14. Sponsoring Agency Code

15. Supplementary Notes

John W. Wilson, Willard R. Weaver, and Donald H. Humes: Langley Research Center, Hampton, Virginia.
Yeunggil Lee: Hampton Institute, Hampton, Virginia. Work performed under NASA Grant NGT-47-020-801.
Ja H. Lee: Vanderbilt University, Nashville, Tennessee. Work performed under NASA Grant NCCI-8.

16. Abstract

A detailed model of the chemical kinetics of the n-C_3F_7I solar-simulator-pumped iodine laser is utilized to study the major kinetic processes associated with the threshold behavior of this experimental system. Excited-state diffusion to the cell wall is the dominant limiting factor below 5 torr. Excited-state recombination with the alkyl radical and quenching by the parent gas control threshold at higher pressures. Treatment of the hyperfine splitting and uncertainty in the pressure broadening are important factors in fixing the threshold level. In spite of scatter in the experimental data caused by instabilities in the simulator high-pressure arc, reasonable agreement is achieved between the model and experiment. Model parameters arrived at are within the uncertainty range of values found in the literature.

17. Key Words (Suggested by Author(s))	18. Distribution Statement
Space power Lasers Chemical Solar laser	Unclassified - Unlimited Subject Category 36

19. Security Classif. (of this report)	20. Security Classif. (of this page)	21. No. of Pages	22. Price
Unclassified	Unclassified	42	A03

For sale by the National Technical Information Service, Springfield, Virginia 22161 NASA-Langley, 1984